Published in IEEE Journal of Selected Topics in Quantum Electronics 13, issue 2, 168-176, 2007
which should be used for any reference to this work

Arrays of High Tilt-Angle Micromirrors for Multiobject Spectroscopy

Severin Waldis, Frederic Zamkotsian, Pierre-Andre Clerc, Wilfried Noell, Michael Zickar, and Nico de Rooij

***Abstract*—Micromirror arrays are promising components for generating reflective slit masks in future multiobject spectrographs. The micromirrors, 100 μm $\times$ 200 μm in size, are etched in bulk single crystal silicon, whereas a hidden suspension is realized by surface micromachining. The micromirrors are actuated electrostatically by electrodes located on a second chip. The use of silicon on insulator (SOI) wafers for both mirror and electrode chip ensures thermal compatibility for cryogenic operation. A system of multiple landing beams has been developed, which latches the mirror at a well-defined tilt angle when actuated. Arrays of 5 $\times$ 5 micromirrors have been realized. The tilt angle obtained is 20° at a pull-in voltage of 90 V. Measurements with an optical profiler showed that the tilt angle of the actuated and locked mirror is stable with a precision of 1 arcmin over a range of 15 V. This locking system makes the tilt angle independent from process variations across the wafer and, thus, provides uniform tilt angle over the whole array. The surface quality of the mirrors in actuated state is better than 10-nm peak to valley and the local roughness is about 1-nm root mean square.**

***Index Terms*—Deep reactive-ion etch (DRIE), micromirror, microoptoelectromechanical system (MOEMS), mirror array, multiobject spectroscopy (MOS).**

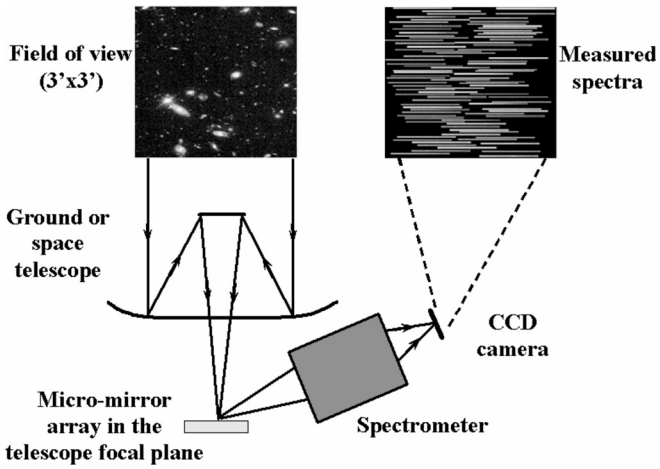

Fig. 1. Principle of a multiobject spectrograph with a micromirror array.

I. Introduction

THE EUROPEAN Cosmic Vision program and the NASA's Origin program bring into fashion what astronomy always wanted to do, explaining our origin by studying the formation of the galaxies and their evolution, as well as the formation and evolution of planets around the nearby stars. Hence, two requirements become a necessity: multiplexing and high spatial resolution capabilities.

Because of its multiplexing capabilities, multiobject spectroscopy (MOS) is becoming the central method to study a large number of objects by simultaneously recording hundreds of spectra and utilizing a target selection mechanism in the field of view. For one of the most central astronomical programs, deep spectroscopic survey of galaxies, the density of objects is low, and it is necessary to probe wide fields of view. The objects of interest have to be selected based on different criteria such as distance, color, and magnitude within deep spectroscopic surveys. This saves time and, therefore, increases the scientific efficiency of observations.

S. Waldis, P.-A. Clerc, W. Noell, M. Zickar, and N. F. de Rooij are with the Institute of Microtechnology (IMT), University of Neuchatel, CH-2007 Neuchatel, Switzerland (e-mail: Severin.Waldis@unine.ch; Pierre-Andre.Clerc@unine.ch; Wilfried.Noell@unine.ch; Michael.Zickar@unine.ch; Nico.deRooij@unine.ch).

F. Zamkotsian is with the Laboratoire d'Astrophysique de Marseille, F-13248 Marseille Cedex 4, France (e-mail: frederic.zamkotsian@oamp.fr).

The remote source-spectra are strongly shifted toward higher wavelengths due to the expansion of the universe (Doppler effect), this is the so-called red-shift effect. Therefore, the spectrographs have to work in the IR wavelengths and, in order to avoid the emission of the "warm" elements at these wavelengths, the instrument must be able to work at cryogenic temperatures inside cryostats for ground-based instruments or in the space environment for space telescopes.

In order to obtain spectra of hundreds of objects simultaneously, future generation of near-IR MOS requires a reconfigurable multislit device (MSD). Conventional masks or complex fiber-optics-based mechanisms could be replaced by microoptical components based on the microelectronics fabrication process, the so-called microoptoelectromechanical systems (MOEMS). MOEMS have produced a wide range of applications such as sensors, switches, microshutters, beam deflectors, and microdeformable mirrors. There are two solutions: micromirror arrays (MMAs) for generating reflecting slits [1], [2] and microshutter arrays (MSA) for generating transmissive slits [3].

Fig. 1 shows the MOEMS-based MOS concept, with MMA as a programmable slit mask. By placing the programmable slit mask in the focal plane of the telescope, the light from selected objects is directed toward the spectrograph ("on" state), while the light from other objects and from the sky background is blocked ("off" state). Any required slit configuration might be obtained with the capability to match point sources or extended

objects. The MMA enables the use of the so-called "long-slit" mode, which astronomers often use with the conventional slit mask. In long-slit mode, a slit longer than the actual size of the studied objects is generated. This is used for the simultaneous recording of both the spectrum of the object and the nearby spectrum of the background; by subtracting the background spectrum, the pure spectrum of the object is finally obtained. A possible MMA candidate would be the digital mirror device (DMD) from Texas Instruments (TI), but this component is not suited for astronomical MOS due to the small size of the micromirrors and the impossibility to work at cryogenic temperatures.

The near-IR multiobject spectrograph (NIRSpec) for the James Webb space telescope (JWST), formerly called next generation space telescope (NGST), is the most advanced instrument project with MOEMS-based slit masks. JSWT, developed by NASA, European Space Agency (ESA), and Canadian Space Agency (CSA) in order to replace the 2.4-m Hubble space telescope, has a primary mirror diameter of 6.5 m and is scheduled to be launched in 2013. This telescope will work in the 0.6–28-μm wavelength band. It will be located at the Lagrange point L2 for a passive cooling down to 35 K. NIRSpec is in realization phase under ESA responsibility. The Laboratoire d'Astrophysiqe de Marseille (LAM) has been involved in all study phases. The selected device is an MSA developed at Goddard Space Flight Center (NASA) [3].

OPTICON is the network, which is consolidating the research efforts of the European astronomical community for next generation instrumentation, especially for the future European extremely large telescope (E-ELT); a Joint Research Activity (JRA) has been set on smart focal planes for developing the components to be used in the focal plane of the telescope for selecting or rearranging the light of the astronomical objects. Within the framework of this JRA, micromirrors have been selected in order to build the first demonstrator of a European MOEMS-based slit mask.

We present in this paper the basic concept of the developed device, its analytical modeling, as well as the finite-element method (FEM) simulation and the fabrication process. Finally, we report on the optical and electromechanical characterization of the first generation devices.

II. Requirements

Over several years, we have developed different tools for the modeling and characterization of these MOEMS-based slit masks, especially during the design studies on JWST-NIRSpec. The models, based on Fourier theory, address two key parameters for the MOS performance: spectral photometric variation (SPV) and contrast. The SPV is an unpredictable photometric variation due to the random distribution of the sources on the slit mask. The SPV requirement is generally $< 10\%$, but as SPV is strongly dependent on the object position and wavelength, the required value cannot be reached. A dithering strategy has been proposed for solving this problem [4]. Contrast is defined as the total amount of nonselected flux of light when the device is set in the "off" position, compared to the amount of light in the "on" position. To avoid spoiler sources (bright stars or galaxies within the instrument field of view) and background to pollute spectra, its value has to be as high as possible. According to the density of objects (stars and galaxies) in the field of view and their magnitude, a contrast requirement of 3000:1 has been established during NIRSpec studies. A characterization bench has been developed for the measurement of these parameters. A DMD made by TI has been used for the first experiments, and contrast values for 10° as well as 20° tilt angles between "on" and "off" position have been measured. The 3000:1 contrast requirement could be fulfilled only with the tilt angle of 20° [5].

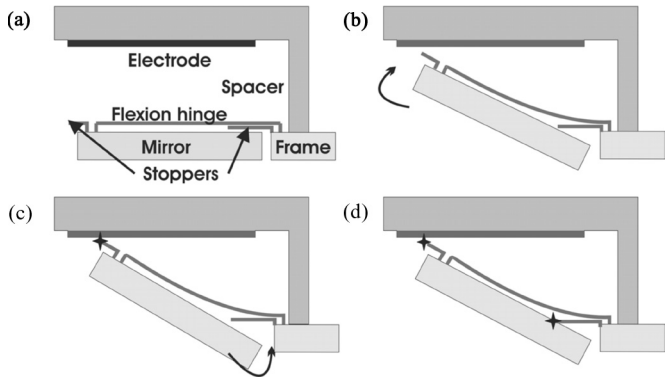

Fig. 2. (a) Schematic view of the basic concept and the electrostatic latching mechanism used to achieve stable tilt angles. (b) and (c) Due to the electrostatic force, the mirror rotates upward until the first stopper beam, which is attached to the mirror, hits the electrode. (d) Then, the mirror starts rotating in the inverse direction until it hits the second stopper beam, which is attached to the mirror frame and remains electrostatically fixed in this position.

The specifications for our MOS micromirrors are partially based on the JWST-NIRSpec studies. The mechanical tilt angle is required to be set at 20° at least. The tilted micromirror is used for the "on" position, and the rest position is considered as the "off" position. Hence, the amount of parasitic light that comes from reflections and scattering of the frame surrounding the micromirrors and of the underneath electrodes can be drastically minimized. A uniform tilt angle must be guaranteed over the whole array in order to send the light through a common pupil in the MOS. The accuracy requirement tilt angle is fixed by the F-number of beams on the array and the admissible oversizing of the pupil in the spectrograph; a reasonable value is 1 arcmin. In the "off" position, the requirement on the mirror location is less accurate as these mirrors send the light back toward the telescope. The mirror surface must remain flat in operation throughout a large temperature range. The impact of the mirror surface quality on the wavefront error budget of the whole instrument is minimized, if the flatness is better than $\lambda/20$. The fill factor of more than 90% is essential, at least along the long slit. One astronomical object is set to fit one mirror. This implies a mirror size of at least 100 μm $\times$ 200 μm, in order to correspond with the plate scale of 8-m-class telescopes as well as the future extremely large telescope (ELT). Future IR instruments for ground-based telescope as well as space telescopes must be cooled down to cryogenic temperatures for background noise reduction. The micromirror array must, hence, work at cryogenic temperatures.

III. Concept

The basic concept of the device is shown in Fig. 2. The micromirrors are actuated electrostatically. Thermal actuation is not suited for IR applications, piezoelectric actuation is not suited due to its small stroke, and magnetic actuation is very complex on system level [3]. The electrostatic actuation combines the required low power dissipation, high stroke, and simplicity on system level. As the device is used as object selector, it is operated in binary mode, i.e., there is an "off" and an "on" state. The flat nonactuated state of the mirrors [shown in Fig. 2(a)] is considered as the "off" state, wherein both the mirror and the electrode are grounded. The pull-in state of the mirror, precisely when the mirror is tilted as shown in Fig. 2(d), is considered as the "on" state.

A single cell of the device consists of a mirror, which is suspended to a supporting frame by a flexible beam, an electrode, and a spacer element that provides a constant gap between the mirror and the electrode. In 2-D arrays, the frame is designed to run along only the long side of the mirror, which makes near-100% fill factor possible along this direction. Stopper beams located on the mirror and on the frame provide tilt-angle control. Physically, the device is realized on two different chips: the mirror chip and the electrode chip. The latter contains the spacer elements.

In order to have mirrors with a planarity better than $\lambda/20$, the mirrors must be sufficiently thick—on the other hand, the mirrors must be as thin as possible to minimize the gap size between the mirrors. The minimal achievable gap size is related to the substrate thickness by the maximum aspect ratio imposed by the etching technology. A gap size as small as possible is desirable for maximizing the fill factor and minimizing stray light originating from below the mirror array. Simulations showed that a thickness of 5 μm is sufficient for the 100 μm $\times$ 200 μm large mirrors to remain flat during the operation. However, a 10-μm-thick substrate has been chosen in order to withstand potential strains originating from the metal coating. Since bare silicon is transparent for IR light, a gold coating on the mirrors is needed for good reflectivity in the IR range. The effect of the metal coating on the mirror planarity can be minimized by using a sandwich-style coating, i.e., coating the front and back side of the mirror with the same thickness of the same material. Thus, potential strains coming from a differential thermal expansion coefficient between gold and silicon are partially compensated for. The flexion-hinge-type suspension is situated on the backside of the mirror. This hidden suspension beam configuration leads to a higher fill factor than lateral suspension beams. As the suspension is covered by the mirror (except for the small gap between the mirror and the frame), we have no stray light coming from the bent beams, which means less degradation of the contrast. The maximum contrast value depends upon the tilt angle of the mirror, which is the angle between the "off" and the "on" state of one mirror. The degradation of the contrast is usually due to the stray light originating from the mirror edges, supporting frame, suspension, and backscattered light from the electrode. As the suspension is hidden by the mirror and the gap size between mirror and frame is small, the degradation of the contrast is mainly due to the rounding of the mirror edges, and surface roughness of the mirror and the frame. The tilt angle is a function of the gap between the electrode and the mirror and the geometry of the suspension. With an intended gap height of 35 μm, tilting angles between 15° and 24° can be achieved. A system of landing posts (or stopper beams) on the mirror and on the frame has been developed to assure a precise and constant tilt angle. This concept is shown in Fig. 2: Once the mirror (i.e., the landing post located on the mirror) touches the electrode, it will not stop moving but will start turning into the opposite direction around this new rotation axis, i.e., the tilting angle tends to decrease once the mirror has landed. This is due to a nonzero (and opposite to the mirror tilting motion) torque around the point where the landing post is attached to the mirror. The reverse turning movement is stopped at a well-defined tilt angle by the stopper beam attached to the frame adjacent to the mirror. The mirror is now electrostatically latched in a position defined by the geometry of the landing posts and the gap between the electrode and the mirror.

The mirror and the electrode chip are fabricated separately on different wafers and then assembled afterward. The mirror chip is made out of a silicon-on-insulator (SOI) wafer. The 10-μm-thick SOI layer (or device layer) is structured into (horizontal) mirrors and frame by bulk micromachining. The optical active side of the mirror is the backside of the device layer, which must be released during fabrication. Intrinsically, the device layer backside is optically flat in terms of roughness and, when released, optically flat in terms of planarity. The suspension structure and the landing posts are realized by surface micromachining of a deposited and doped polycrystalline silicon layer underneath the mirror and frame. Polysilicon is used rather than any other material, as it has a thermal expansion coefficient similar to single crystal silicon. This is important for the operation in cryogenic environment. In order to assure thermal expansion compatibility with the mirror chip, the electrode chip is also based on an SOI wafer. Beside the electrodes, connecting lines, and connecting pads, the electrode chip also contains the spacer elements, which ensure a constant gap between the electrode and the mirror chip. The spacer height is fixed and defined by the thickness of the device layer of the electrode chip, therefore the uniformity of the spacer height (and the uniformity of tilt angle) depends on the uniformity in thickness of this silicon layer.

IV. Modeling

The required mechanical tilt angle of the MOS micromirrors is 20°. For this given tilt angle, we want to minimize the required gap height, i.e., the spacing between the mirror and the electrode. This for the following reasons.

1) For a given geometry of the flexure beam, the actuation voltage is proportional to the gap height.
2) The present actuator architecture implies that a part of the tilted mirror ("on" state) is optically blocked from the adjacent frame. This covering reduces the operational fill factor. It can be minimized by minimizing the gap height.

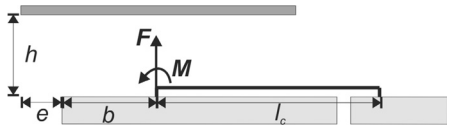

Fig. 3. Suspension model. The electrostatic forces acting on the mirror are replaced by a resulting force and moment acting on the endpoint of the suspension cantilever.

3) The crosstalk between two adjacent mirrors depends upon the gap height; the smaller the gap height, the less pronounced the crosstalk.

In this section, we discuss the effects of the suspension and stopper geometry and electrode position on the behavior of the actuator.

The dimensions of the flexion beams are determined by the constraint on the resonance frequency, actuation voltage, and the maximum allowable stress. The only degrees of freedom to influence the tilt-angle-per-gap-height ratio are the suspension attachment offset (parameter b in Fig. 3) and the relative position of the electrode (parameter e in Fig. 3).

We consider the case of a cantilever suspension as shown in Fig. 3. Assuming a thin (i.e., width $\gg$ thickness) cantilever, we can neglect the in-plane movement of the mirror and can consider only the movement in the plane perpendicular to the mirror. Furthermore, if we consider that the mirror is much thicker and larger than the cantilever, we can assume the mirror to be rigid.[1] The electrostatic forces acting on the mirror can then be reduced to a resulting force and moment acting on the point where the cantilever is attached to the mirror, as shown in Fig. 3. The resulting piston movement and tilt angle due to the force F and the moment M is obtained by linear superposition, i.e., summation of the two individual contributions. Considering small deflections, thee y-deflection of the cantilevers end can be stated as

$$\begin{aligned}\delta &= \delta_F - \delta_M \\ &= \frac{l_c^2}{EI_y}\left(\frac{Fl_c}{3} - \frac{M}{2}\right)\end{aligned} \tag{1}$$

and of the angle as

$$\begin{aligned}\alpha &= \alpha_F - \alpha_M \\ &= \frac{l_c}{EI_y}\left(\frac{Fl_c}{2} - M\right)\end{aligned} \tag{2}$$

where l_c is the cantilever length, E is the Young's modulus, and I_y is the moment of inertia around the y-axis [6]. The moment of inertia is given with $I_y = wd^3/12$, where w is the width of the cantilever and d the thickness. The (vertical) piston movement of the mirror is represented in 1, whereas 2 represents the tilt angle. Note that the ratio α/δ [obtained from 1 and 2] decreases with the length of the cantilever l_c. It is obvious from 2 that for a mirror motion as shown in Fig. 2(b), we must have $Fl_c > 2M$. If we have $Fl_c < 2M$, the mirror tilts in the opposite direction. The relation between F and M depends on the suspension attachment offset b and the relative position of the electrode to the mirror e. Now, consider $b = 0$ and the electrostatic pressure on the mirror as p_E where the electrode covers the mirror, and 0 otherwise. The resulting moment can then be stated as

$$M = p_E \frac{(l_m - e)^2}{2} \tag{3}$$

and the resulting force as

$$F = p_E(l_m - e). \tag{4}$$

It follows immediately that for $l_m = l_c$ and $e = 0$, the angle α is zero. Thus, we need an asymmetry either in the electrode positioning or flexion beam geometry for optimum performance of the device. The optimum positioning of the electrode depends on the positioning of the flexion beam. Now, considering $e = 0$, $b \neq 0$, and the electrostatic pressure $p = F/l_m$, the resulting force would then be F and the resulting moment would be

$$\begin{aligned}M &= \int_{-b}^{0} \frac{F}{l_m} x\, dx + \int_{0}^{l_m} \frac{F}{l_m} x\, dx \\ &= \frac{l - 2b}{2} F.\end{aligned} \tag{5}$$

By combining 1–5, we can predict the mirror angle and piston in function of the cantilever attachment offset b. For small angles, the gap height equals $\delta + b\alpha$. Putting $l_m = l_c = l$, the tilt-angle *versus* gap-height ratio can be

$$\frac{\alpha}{\delta + \alpha b} = \frac{b}{b^2 + \frac{l}{2}b + \frac{l^2}{12}} \tag{6}$$

The normalized function is plotted in Fig. 4. We note a strong dependence of the tilt-angle-per-gap-height ratio on the positioning of the flexion beam attachment point. The maximum value occurs at $b = l/\sqrt{12}$.

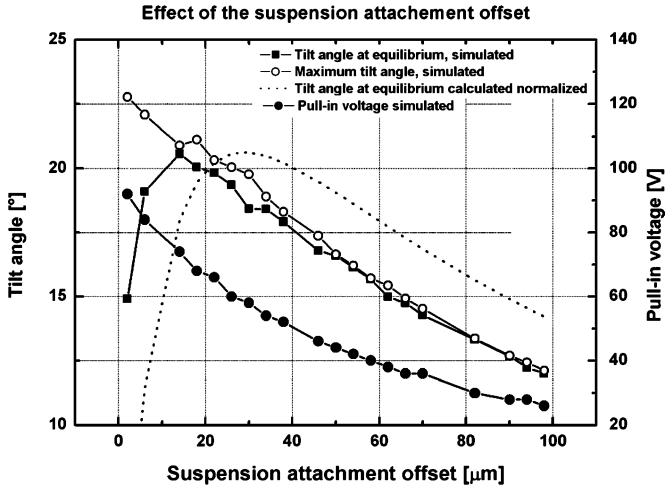

Fig. 4. Tilt angle and pull-in voltage *versus* suspension offset b for a gap height $h = 35\ \mu$m and flexion beam dimensions $d = 0.5\ \mu$m, $w = 10\ \mu$m, and $l_c = 100\ \mu$m. For comparison, a normalized plot of the analytic formula for the pull-in voltage is drawn (dashed curve).

[1]The deflection δ due to a force F of a beam with rectangular section wh can be written as $\delta \sim F/wh^3$ Assuming a beam with 10 μm $\times$ 0.5 μm section and a mirror with a 200 μm $\times$ 10 μm section, having the same length, a force F would deflect the mirror $20^4 = 160\,000$ times less than the cantilever.

Considering the real case, where large deflections and large angles occur, simulations using the FEM must be carried out. Large out-of-plane movements, especially tilting movements, often cause convergence problems in coupled electrostatic and mechanical simulation due to strong mesh deformation and nonlinearity. Nonlinearity occurs due to stress-stiffening, which must be taken into account when considering large deflections of the cantilever that cannot be avoided. Mesh deformation can be avoided by remeshing the electrostatic and mechanical model after each iteration. Thus, we developed a script-based custom 2-D electromechanical model for use with ANSYS. The principal idea is to separate the mechanical and electrostatic model. The electrostatic model calculates the forces that act on the mirror; the resulting force and moment is then transferred onto the cantilever in the mechanical model. The simulation of the mechanical model then gives the deflection of the cantilever and the new position of the mirror, which is again transferred into the electrostatic model. For each iteration, the electrostatic model is rebuild and remeshed based on the geometrical data calculated by the mechanical (cantilever) model. Simulations were carried out by varying the key parameters of the micromirror device: cantilever geometry, cantilever position, electrode position, and gap height. Tilt angle, pull-in voltage, maximum stress, and the first resonance frequency were extracted from the simulations. The first resonance frequency, which is a measure for shock resistance, is between 800 Hz and 2 kHz for different designs, which is an acceptable range for the considered application. The maximum stress in the cantilever ranges from 120 to 400 MPa. The upper limit of 400 MPa is imposed for the reliability of the polysilicon suspension. The fracture strength of polysilicon is reported to be a few gigapascals [7]; however, this threshold may be lowered during postprocessing and also, stresses may locally be higher in reality than in simulation. From our experience, we consider 400 MPa to be an upper limit for safe operation. Based on these simulations, we set the dimensions of the cantilever to be 70–100 μm in length, 0.3–0.6 μm in thickness, and 3–7 μm in width. The gap height is set as 35 μm.

For studying the influence of the electrode position and the cantilever attachment point on the tilt-angle-per-gap-height ratio, we fixed the gap height and searched the highest tilt angle for this given gap. This comes to the same as minimizing the gap height for a given tilt angle because, as the simulation confirmed, the tilt angle goes linear with the gap height for a given configuration. We found that there is indeed a maximum tilt angle in function of the positioning of the electrode (parameter e), although it is not very pronounced. The position of the maximum depends upon the cantilever attachment offset b; by increasing b, e decreases. We set $e = l_m/10$, which corresponds to the ideal position for $b = l_m/5$.

The dependency of the tilt angle (for a given gap and a given electrode offset) is shown in Fig. 4. First, consider the tilt angle at equilibrium, which is the position where the mirror is in steady state, at the indicated pull-in voltage and without the stopper beam system. Note that the simulated curve has the same shape as the calculated curve, but its maximum is shifted. This is due to the shifted electrode ($e = l_m/10$) used for the simulation. If we look at the evolution of the tilt angle rather than the steady state, we note that the tilt angle reaches a maximum value, before the mirror is settled in the steady state. This result confirms the hypothesis made for the latching system showed in Fig. 2(c): Once the mirror hits the electrode, it starts to rotate in the inverse direction decreasing its tilt angle. In order to have the mirror latched as proposed in Fig. 2(d), the geometry of the stopper beams must be chosen such that they stop the mirror between the maximum and the equilibrium tilt angle. The range between the maximum and the steady-state value can be considered as the tuning range of the tilt angle for a given gap height. One could, by augmenting the actuation voltage beyond the pull-in voltage, extend this range, i.e., lower the steady-state value. However, this is not suited for our application as we intend to use a hold voltage lower than the pull-in voltage. Ideally, the stopper beams are adjusted such that the mirror is stopped shortly after reaching the maximum tilt angle. This way, the useable range for the hold voltage is maximized. We remark that the difference between the maximum and the steady-state tilt angle decreases strongly with increasing b. The absolute value of the maximum achievable tilt angle also decreases with increasing b. Thus, for a maximum tilt-angle-per-gap-height ratio and for a maximum tuning range, we chose $0\,\mu\text{m} \leq b \leq 20\,\mu\text{m}$. The geometry, i.e., the length of the stopper beams is chosen such that the mirror is stopped at an angle 10% of the tuning range below the maximum value. This margin accounts for process variations. That way, the proper function of the latching mechanism and, thus, the uniform tilt angle is assured. The uniform tilt-angle condition is a crucial requirement for the mirror array to be used in an MOS system.

V. Fabrication

Arrays of 2×2 and 5×5, as well as single mirrors with either flexion or torsion beam suspension and different types of electrodes have been fabricated. Mirror sizes of 100 μm $\times$ 200 μm, 200 μm $\times$ 100 μm, and 250 μm $\times$ 500 μm have been implemented. Flexion and torsion beams with various lengths and widths, and a thickness of 0.6 μm have been realized. The fabrication includes the processing of the mirror wafer, the processing of the electrode wafer, and the assembly of the released mirror chips and diced electrode chips. Fig. 5 shows the fabrication process of the mirror chip. The 10-μm-thick device layer of an SOI wafer is structured into the mirrors and the frame by deep reactive-ion etching (DRIE). At the same time, the trenches for the dice free release [8] have been defined. During the next step, 2.2 μm thermal wet silicon dioxide is grown in order to fill the trenches between the mirrors and the frame. Reactive-ion etching (RIE) is used afterward to open the SiO_2, where the suspension is attached to the mirrors and the frame. A polysilicon layer is then deposited by chemical vapor deposition (CVD) and doped. Then, the suspension and the landing posts are structured into the polysilicon layer. DRIE has been used, in order to preserve the dimensions of the fine polysilicon structures to the maximum extent. A slight overetch is necessary here to avoid polysilicon residues, which are located in the dips created during gap refill. In a final DRIE step, the backside openings of

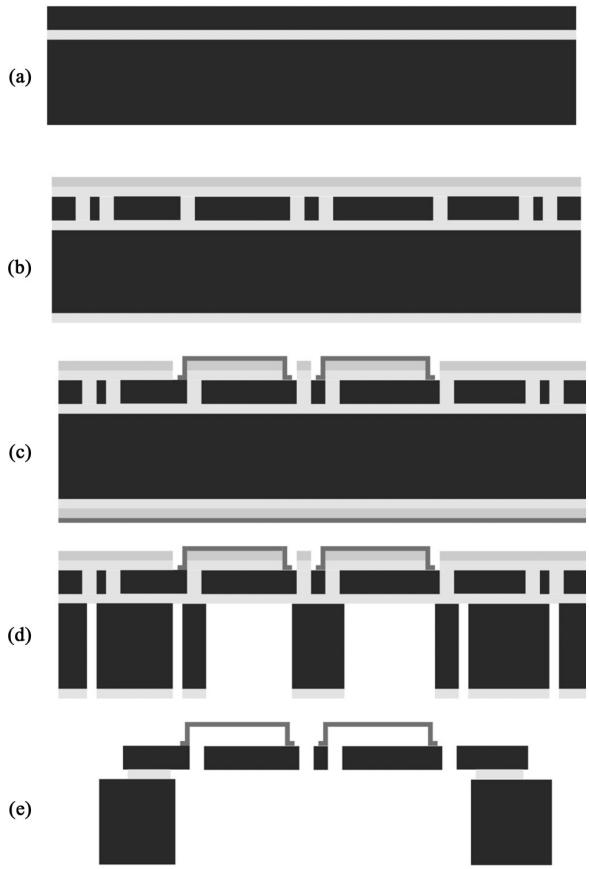

Fig. 5. Process flow mirror chip. (a) SOI wafer with a 10-μm-thick device layer is used as substrate. (b) Mirrors and frame are defined by DRIE, the gaps are filled by oxidation. (c) Oxide is opened by RIE at the points of attachment of the suspension and the landing posts, deposition by CVD, and structuring by DRIE of the polysilicon layer. (d) Opening of the mirrors by backside DRIE. (e) HF vapor release of the mirrors and the chips.

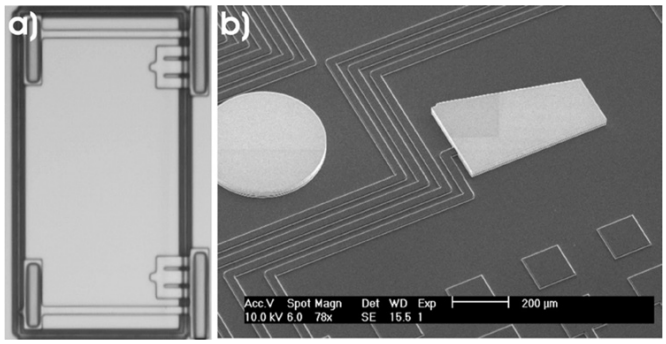

Fig. 6. Fabrication results. (a) Optical microscope image of the suspension side of a microfabricated single mirror. The size of the mirror is 100 μm $\times$ 200 μm. The mirror is suspended by two cantilever flex hinges. The extra pads at the top will be used for the electrostatic latching mechanism. (b) Scanning electron microscope close-up view of the fabricated electrode chip. The structures in white are the integrated spacer elements, which also serve to passively align the micromirror chip in the assembly step.

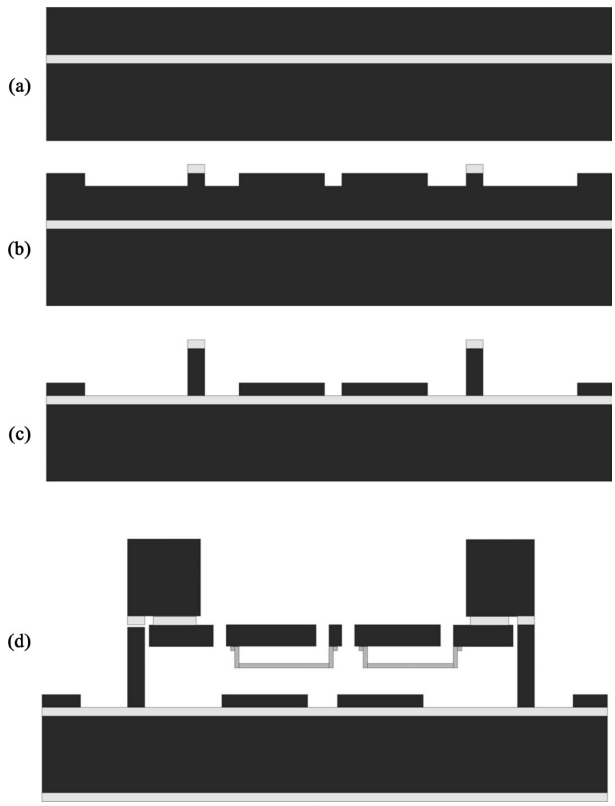

Fig. 7. Electrode chip. (a) SOI wafer with a 50-μm-thick device layer is used as substrate. (b) Definition of spacers (protected by an oxide mask) and electrodes by a first DRIE step. (c) Transfer of the electrode pattern to the bottom of the device layer by a second DRIE step. (d) Mirror chip is put on the spacers of the electrode chip and aligned.

the mirror and the dice free chip release trenches are etched into the 350-μm handle layer. First, the mirrors and then, the whole chips are released in a dry hydroflouro (HF) vapor etch step [8]. The mirror chips are now ready to be assembled with the electrode chip. Fig. 6(a) shows a micrograph of a released single mirror with flexion suspension. The sandwich-style thin film reflective coating used for IR operation is currently under development.

Fig. 7 shows the fabrication process of the electrode chip. An SOI wafer with a 50-μm-thick device layer is patterned using a self-aligned delay mask process [9]. In the first step, a 0.5-μm-thick thermal silicon dioxide is grown. In the first photolithography and subsequent RIE step, the spacer mask is coarsely defined in the oxide mask. In the second photolithography and RIE step, the precise form of the spacer is defined in the oxide mask, and at the same time the electrodes, connection pads, and connecting lines are patterned into photoresist. Then, by using time-controlled DRIE, the first couples of micrometers are etched. This step defines the height of the electrodes and connecting lines. After oxygen plasma resist strip, the remaining thickness of the device layer is etched. In that way, the electrode and the connecting lines pattern is transferred to the bottom of the device layer, while the spacers, protected by a silicon dioxide mask, still have the initial height of the device layer. In the final step, the wafer is diced to obtain the individual electrode chips. Fig. 6(b) shows a closeup of the electrode chip ready for assembly. The electrodes of the first run showed heights ranging from 4 to 15 μm, and the spacers showed a height of 48 μm. Within one chip, the variation of the electrode height is smaller than 100 nm and the variation of the spacer height is smaller than 10 nm.

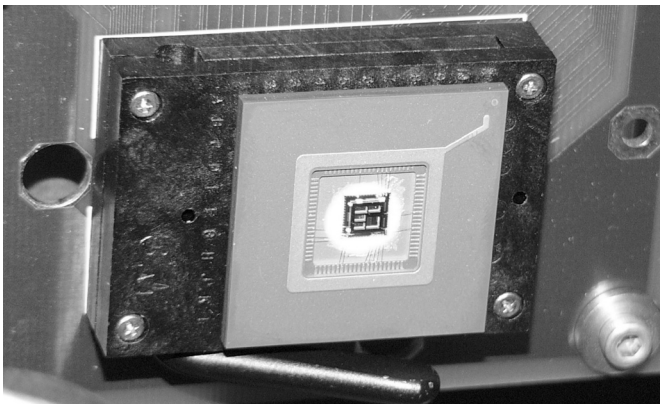

Fig. 8. Assembled and packaged device mounted on a custom PCB.

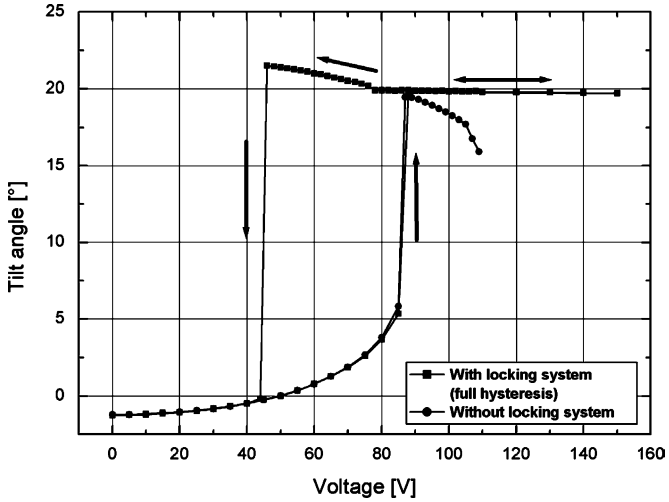

Fig. 9. Tilt angle *versus* voltage hysteresis. The mirror with the landing beam mechanism is electromechanically latched at 20°. The angle remains stable within 1 arcmin over a range of 15 V around the pull-in voltage.

The last fabrication step is the assembly of the electrode and the mirror chip (Fig. 7(d)). The mirror chip is placed upside down on the angled quad spacers of the electrode. The mirror chip is then pushed parallel to the angled squads. The angled squads, with their counterparts on the mirror chip, guide the mirror chip to a good position. Once the electrodes and the mirrors are aligned, a clipping system on the mirror chip snaps in and holds the mirror in the aligned position. The alignment error is below 5 μm. The clipping system holds the device together under moderate accelerations, but for durable assembly, the chip is fixed with conductive silver glue. The assembled device is packaged and wire bonded in a PGA84 housing. A printed circuit board (PCB) equipped with a grid zip connector is used for easy mechanical and electrical interfacing. Fig. 8 shows the assembled and packaged device mounted on the grid zip socket.

VI. Characterization

A dedicated characterization bench has been developed for the complete optoelectromechanical analysis of MOEMS devices, actuators, or micromirrors as well as full arrays. This modular Twyman–Green interferometer allows high in-plane resolution (3 μm) or large field of view (40 mm). Out-of-plane measurements are performed with phase-shifting interferometry showing very high resolution (standard deviation < 1 nm). Features such as optical quality or electromechanical behavior are extracted from these high-precision 3-D component maps. The range is increased without loosing accuracy by using two-wavelength phase-shifting interferometry authorizing measurements of large steps [10]. All measurements have been confirmed with a Veeco/Wyko NT1100 Dynamic MEMS (DMEMS) optical profiler.

Electromechanical actuation tests showed the basic functionality of the device. The mechanical properties of the micromirrors did not change after 10^6 operations, i.e., the device remained functional and the actuation voltage required to switch the mirror in the "on" state remained constant. The mirrors showed a slight negative residual tilt of 1° to 2° after fabrication. This may be due to a stressed polysilicon–silicon interface, or due to a stress gradient within the deposited polysilicon layer.

The surface quality of uncoated mirrors was measured in the "off" and the "on" state. The 100 μm $\times$ 200 μm mirrors showed a peak-to-valley deformation of 7 nm, in "on" and in "off" position. As predicted, the mirrors remain flat when operated. The flatness of the mirror is required to be $\lambda/20$ for $\lambda \geq 1\,\mu$m, which gives 50 nm. Thus, our mirror quality is easily within the specifications. Larger mirrors of 250 μm $\times$ 500 μm, which may be used for larger telescopes, showed a PTV of 15 nm, still satisfying the requirement of optical flatness. The local roughness is comparable to an unprocessed silicon wafer, which is around 1-nm root mean square (rms).

The mechanical tilt angle, in function of the applied voltage, has been measured for different designs of the suspension and stopper geometry. First, the applied voltage is increased up to the pull-in point (at 90 V) or "on" state (and beyond). The tilt angle at the pull-in voltage equals the tilt angle at equilibrium, as exhibited in Section IV. From this point onward, the voltage is decreased until the mirror snaps back to the "off" position. The tilt-angle value at which the mirror snaps back, is equal to the maximum tilt angle of the mirror during the transition from the "off" to the "on" state,[2] as simulated in Section IV. The resulting tilt angle *versus* voltage hysteresis is plotted in Fig. 9, for two mirrors with a suspension attachment offset $b = 20\mu$m: one mirror equipped with the stopper beams and one mirror, serving as reference, without stopper beams. We observe that the maximum tilt angle and the equilibrium tilt angle are in good agreement with the simulated values: For a suspension attachment offset $b = 20$ μm, we have from Fig. 4 a maximum tilt angle of 21° (21.6° measured) and an equilibrium tilt angle of 20° (19.8° measured). Furthermore, the flat region around the pull-in point of the mirror with the stopper beams proves

[2]This is true, as both simulation and measurement consider quasistatic cases. Considering the real dynamic transition between the "off" and the "on" state, the maximum tilt angle and the snap-back tilt angle might not be exactly the same. So far, we have not succeeded either in measuring or in simulating the dynamic transition.

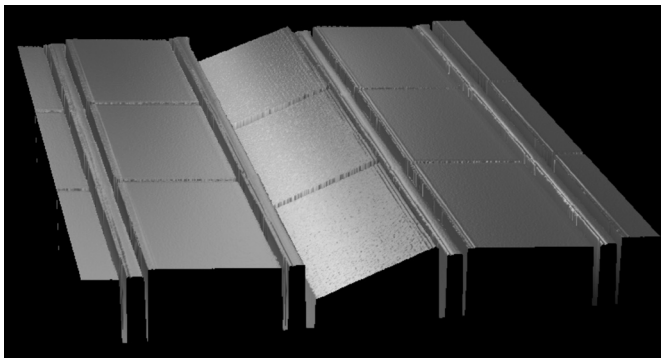

Fig. 10. 3-D optical profiler image showing a 3×3 subset of a 5×5 micromirror array. One row is actuated, implementing the long-slit mode. The fill factor is 97% along the slit.

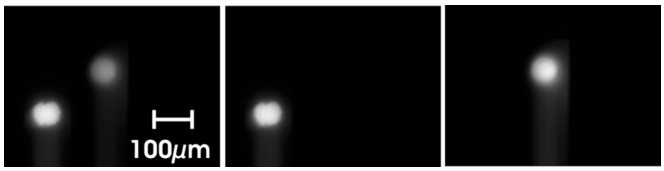

Fig. 11. CCD images corresponding to the imaging plane of the spectrometer. In the first image, two objects are present in the field of view, in the second and third image, one out of the two objects is selected, blocking completely the light of the other object. The projected object has a diameter of 50 μm.

the latching mechanism. The stopper beams hold the mirror in a stable position. Precisely, the tilt angle remains stable within 1 arcmin over a voltage range of 15 V. This way, process variations that are translated into a variation of the tilt angle for a given voltage, can be suppressed. Thus, the uniformity of the tilt angle over large arrays will merely depend on a uniform spacing between the micromirrors and the electrodes. A multicolumn system guaranteeing uniform spacing over large areas is currently under development.

A dedicated setup, which simulates the field of view of a telescope, was used to demonstrate the capabilities of the device for object selection. The field of view, in our case, consists of two objects (e.g., galaxies) and is situated on two different arms of the optical setup. These objects are imaged on the 5×5 micromirror array, which is again imaged by a charge coupled device (CCD) camera, simulating the spectrograph function. In a real MOS system, the spectrograph would be at the place of the CCD camera. The long-slit mode is used to select either one or the other object in the field of view. Fig. 10 illustrates the long-slit mode, i.e., all five mirrors in a line of the 5×5 micromirror array are tilted at the same time. Note that the fill factor along the slit is is very high, i.e., 97%. First, both objects are selected, that is the mirror lines where the object is projected on are tilted. Then, simultaneously, only either the right or the left object is selected. Fig. 11 shows the series of images as seen by the CCD camera (spectrograph).

VII. Conclusion

The presented device mostly fulfils the key parameters for use in future multiobject spectrographs. It features optical flat mirrors that can be tilted by 20° with an actuation voltage below 100 V. A system of multiple landing posts, which provides a uniform tilt angle has been demonstrated. The long-slit mode, featuring 97% fill factor along the slit, has been used to demonstrate object selection. Currently, large micromirror arrays of up to 100×200 mirrors are being fabricated. To cope with this large number of actuators, we develop a column-line addressing scheme, which reduces the number of driving voltages from n^2 to $2n$ and through-wafer interconnects. The construction of a cryogenic chamber is under way, which allows a complete opto-electromechanical characterization of the device in a cryogenic environment.

Acknowledgment

We gratefully acknowledge the COMLAB staff at the joint microfabrication facility of IMT and CSEM and P. Lanzoni at LAM for his valuable support during device characterization.

References

[1] F. Burg, P. Bely, B. Woodruff, J. MacKenty, M. Stiavelli, S. Casertano, C. McCreight, and A. Hoffman, "Yardstick integrated science instrument module concept for NGST," in *Proc. SPIE Conf. Space Telesc. Instrum. V*, Kona, HI, 1998, vol. 3356, pp. 98–105.

[2] F. Zamkotsian, K. Dohlen, D. Burgarella, and V. Buat, "Aspects of MMA for MOS: Optical modeling and surface characterization, spectrograph optical design," in *Proc. NASA Conf. NGST Sci. Technol. Expo.*, Hyannis, MA, 1999, vol. 207, pp. 218–222.

[3] S. H. Moseley, R. Arednt, R. A. Boucarut, M. Jhabvala, T. King, G. Kletetschka, A. S. Kutyrev, M. Li, S. Meyer, D. Rapchun, and R. S. Silverberg, "Microshutters arrays for the JWST near infrared spectrograph," in *Proc. SPIE*, vol. 5487, pp. 645–652.

[4] F. Zamkotsian and K. Dohlen, "Performance modeling of JWST near infrared multi-object spectrograph," in *Proc. SPIE Conf. Astron. Telesc. Instrum.*, Glasgow, U.K., 2004, vol. 5487, pp. 635–644.

[5] F. Zamkotsian, J. Gautier, and P. Lanzoni, "Characterization of MOEMS devices for the instrumentation of next generation space telescope," in *Proc. SPIE Conf. MOEMS*, San Jose, CA, 2003, vol. 4980, pp. 324–332.

[6] W. C. Young, *Roark's Formulas for Stress and Strain*, 8th ed. New York: McGrawHill, 1989.

[7] H. Kapels, R. Aigner, and J. Binder, "Fracture strength and fatigue of polysilicon determined by a novel thermal actuator," in *IEEE Trans. Electron Devices*, vol. 47, no. 7, pp. 1522–1528, Jul. 2000.

[8] T. Overstolz, P. A. Clerc, W. Noell, M. Zickar, and N. F. de Rooij, "A clean wafer-scale chip-release process without dicing based on vapor phase etching," in *Proc. 17th IEEE Int. Conf. Micro Electro Mech. Syst.*, Maastricht, The Netherlands, 2004, pp. 717–720.

[9] S. Kwon, V. Milanovic, and L. P. Lee, "Large-displacement vertical microlens scanner with low driving voltage," *IEEE Photon. Lett.*, vol. 14, no. 11, pp. 1572–1574, Nov. 2002.

[10] A. Liotard, S. Muratet, F. Zamkotsian, and J. Fourniols, "Static and dynamic microdeformable mirror characterization by phase-shifting and time-averaged interferometry," in *Proc. SPIE Conf. MOEMS*, 2005, vol. 5716, pp. 207–217.

Severin Waldis was born in Berne, Switzerland, on April 15, 1978. He received the Diploma in physical electronics from the University of Neuchatel, Neuchatel, Switzerland, in 2004, where he is currently working toward the Ph.D. degree at the Institute of Microtechnology.

His current research interests include micromirror arrays based on a combination of bulk and surface micromachining.

Frederic Zamkotsian received the Ph.D. degree in physics from the University of Marseilles, Marseilles, France, in 1993.

Since 1998, he has been with the Laboratoire d'Astrophysique de Marseille, Marseille, where he is responsible for the development of new MOEMS devices for future astronomical instrumentation, in collaboration with microtechnology laboratories in Europe. His current research interests include conception and characterization of programmable slit masks for multiobject spectroscopy (JWST, European networks) and microdeformable mirrors for adaptive optics (ELT, European networks).

Pierre-Andre Clerc received the Diploma in process engineering from the Technical School of La-Chaux-de-Fonds, Switzerland, in 1978

Since 1989, he has been a Process Engineer with the Institute of Microtechnology, University of Neuchatel, Neuchatel, Switzerland, where he is responsible for the plasma etching technology.

Wilfried Noell received the Ph.D. degree in physics from the University of Ulm, Germany, in 1998.

Since 1998, he has been with the Institute of Microtechnology, University of Neuchatel, Neuchatel, Switzerland, where he is responsible for the group's activities on optical microsystems.

Michael Zickar was born in Pompaples VD, Switzerland, on February 15, 1977. He received the Ph.D. degree from the University of Neuchatel, Neuchatel, Switzerland, in 2006.

He cofounded Idonus Sarl, a company specialized in instruments for wet- and vapor- phase etching apparatuses for microfabrication, in 2004. He is currently a Postdoctoral Researcher at the Institute of Microtechnology, University of Neuchatel. His current research interests include optical crossconnects and microelectromechanical systems for medical devices.

Nico de Rooij (F'02) received the M.Sc. degree in physical chemistry from the State University of Utrecht, The Netherlands, in 1975, and the Ph.D. degree from Twente University of Technology, The Netherlands, in 1978.

From 1978 to 1982, he was with the Research and Development Department of Cordis Europa The Netherlands. He joined the Institute of Microtechnology of the University of Neuchatel, Neuchatel, Switzerland (IMT UNI-NE), as a Professor and the Head of the Sensors, Actuators and Microsystems Laboratory in 1982. From October 1990 to October 1996, and again from October 2002, he was the Director of the IMT UNI-NE. Since 1989, he has been a part-time Professor with the Swiss Federal Institute of Technology, Lausanne, Switzerland. His research interests include microfabricated sensors, actuators, and microsystems.

Prof. Rooij was a member of the steering committee of the International Conference on Solid-State Sensors and Actuators and of Eurosensors. He was the European Program Chairman of Transducers'87 and the General Chairman of Transducers'89. He is a member of the Editorial Boards for the journals *Sensors and Actuators, Sensors and Materials* and the IEEE JOURNAL OF MICROELECTROMECHANICAL SYSTEMS.